

MULTI-MODAL ROBUST ENHANCEMENT FOR COASTAL WATER SEGMENTATION: A SYSTEMATIC HSV-GUIDED FRAMEWORK

Zhen Tian¹, Christos Anagnostopoulos^{1,*}, Qiyuan Wang¹, Zhiwei Gao²

¹ School of Computing Science, University of Glasgow

² School of Computing Engineering, University of Glasgow

ABSTRACT

Coastal water segmentation from satellite imagery presents unique challenges due to complex spectral characteristics and irregular boundary patterns. Traditional RGB-based approaches often suffer from training instability and poor generalization in diverse maritime environments. This paper introduces a systematic robust enhancement framework, referred to as Robust U-Net, that leverages HSV color space supervision and multi-modal constraints for improved coastal water segmentation. Our approach integrates five synergistic components: HSV-guided color supervision, gradient-based coastline optimization, morphological post-processing, sea area cleanup, and connectivity control. Through comprehensive ablation studies, we demonstrate that HSV supervision provides the highest impact (0.85 influence score), while the complete framework achieves superior training stability (84% variance reduction) and enhanced segmentation quality. Our method shows consistent improvements across multiple evaluation metrics while maintaining computational efficiency. For reproducibility, our training configurations and code are available here ¹.

Index Terms— Semantic segmentation, Coastline detection, HSV color space, robust training, Physics-informed multi-objective learning.

1. INTRODUCTION

Coastal water segmentation from satellite and aerial imagery is a core task in remote sensing, with applications in environmental monitoring, climate studies, and coastal management [1]. Traditional RGB-based methods struggle in maritime scenes due to spectral variability, atmospheric effects, and complex shorelines [2, 3, 4]. Deep learning methods, especially U-Net variants, achieve strong results in semantic segmentation [5]. However, for coastal waters, they face several issues: (1) unstable training from class imbalance and spectral similarity, (2) weak boundary detection in complex coasts, (3) false positives in deep sea, and (4) unrealistic coastline connectivity [6, 7, 8, 9, 10, 11].

Our key idea is that water bodies show clear patterns in the HSV color space [12], with lower saturation and stable hue ranges across lighting and water types. In addition, coastal boundaries follow geometric rules that can guide segmentation. Our contribution is summarized as follows:

- We prove that each loss component is Lipschitz continuous, and that the composite objective ensures convergence of gradient descent (Theorem 1 in Section 3.2), thereby guaranteeing reliable optimization.
- We show that these spectral–geometric constraints shrink the effective hypothesis space (Theorem 2 in Section 3.2), providing theoretical support for their stabilizing role in water–land separation.
- We provide comprehensive experiments that demonstrate clear performance gains over state-of-the-art baselines in both stability and boundary accuracy.

2. RELATED WORK

2.1. Deep Learning for Water Segmentation

Traditional water segmentation methods relied on spectral indices such as NDWI and MNDWI [13, 14]. With the advent of deep learning, convolutional neural networks have become the dominant approach. U-Net [15] and its variants have shown particular success in biomedical and remote sensing applications. Recent works have explored various architectural improvements including attention mechanisms [16], multi-scale fusion [17], and encoder-decoder enhancements. However, most approaches ignore addressing the fundamental challenges of color space representation and training stability.

2.2. Color Space Utilization

While RGB remains the standard representation, alternative color spaces have demonstrated advantages in specific applications. HSV color space has been successfully applied in object tracking [18], and agricultural monitoring [19]. However, its systematic integration into deep learning frameworks for water segmentation remains underexplored.

* Corresponding Author

¹<https://github.com/UofgCoastline/ICASSP-2026-Robust-U-net>

2.3. Robust Training in Semantic Segmentation

Training stability in semantic segmentation has gained attention due to gradient instability and convergence issues. Various regularization techniques including label smoothing, focal loss, and consistency training have been proposed. Our work differs in that we explicitly integrate spectral priors using HSV-based supervision and geometric constraints into the training objective. Unlike generic regularization, these domain-informed components reduce the effective hypothesis space and enforce spatial coherence, leading to more stable and interpretable convergence, as will be shown in our evaluation.

3. METHODOLOGY

We introduce a novel framework, coined Robust U-Net, for robust coastline delineation that integrates physics-informed supervision, geometric regularization, and regional consistency enforcement. Robust U-Net is grounded in two fundamental theoretical properties that ensure convergence guarantees and hypothesis space reduction, providing both theoretical rigor and practical effectiveness for coastal boundary extraction in satellite imagery.

3.1. Overview

Let $\mathbf{I} \in \mathbb{R}^{H \times W \times 3}$ be an input satellite image of dimensions $H \times W$ with three RGB channels. Our objective is to learn a mapping $f_\theta : \mathbb{R}^{H \times W \times 3} \rightarrow [0, 1]^{H \times W}$ parameterized by θ , which produces a water probability mask $\mathbf{M} = f_\theta(\mathbf{I})$, where M_{ij} represents the probability that pixel (i, j) belongs to a water region. Our methodology achieves robust coastline delineation through a synergistic design of multiple loss components and post-processing, formulated as a unified optimization problem that balances semantic accuracy, spectral consistency, geometric regularity, and spatial coherence.

3.2. Theoretical Guarantees

We provide two theoretical results that formalize the robustness of our framework. The first establishes the convergence properties of our composite loss, while the second demonstrates how spectral and geometric priors reduce the effective hypothesis space. Proof sketches are provided below; full technical details of the proofs are omitted due to space limitations.

Theorem 1 (Convergence Guarantee). *Each component loss \mathcal{L}_i in our framework is Lipschitz continuous with constant L_i , ensuring that the composite objective satisfies*

$$\|\mathcal{L}_{Robust}(\mathbf{M}_1) - \mathcal{L}_{Robust}(\mathbf{M}_2)\| \leq L \|\mathbf{M}_1 - \mathbf{M}_2\| \quad (1)$$

where $L = \max_i \lambda_i L_i$ and λ_i are the loss balancing coefficients. This guarantees convergence of gradient descent to a stationary point at rate $O(1/\sqrt{T})$, for T iterations.

Sketch of Proof. The result follows from the Lipschitz continuity of each \mathcal{L}_i , which ensures bounded gradient differences. The composite objective inherits Lipschitz continuity with constant $L = \max_i \lambda_i L_i$. By standard convergence analysis of stochastic gradient descent on Lipschitz-continuous non-convex objectives [20], this leads to $O(1/\sqrt{T})$ convergence to a stationary point. Due to space limitations, we omit the full technical details. \square

Theorem 2 (Hypothesis Space Reduction). *The combined influence of spectral priors and geometric regularizers reduces the effective hypothesis space according to*

$$\mathcal{H}_{Reduced} \approx \rho \cdot \mathcal{H}_{Full} \quad (2)$$

where $\rho \propto \text{Corr}(\text{HSV features, true water labels})$ quantifies the correlation between HSV-based indicators and ground truth water labels, and $\text{Corr}(\cdot)$ denotes statistical correlation.

Sketch of Proof. Domain-informed priors act as additional inductive bias, constraining the hypothesis space to models consistent with spectral and geometric properties. Formally, introducing constraints K yields a reduced space $H' = \{h \in H : h \models K\}$ with $H' \subseteq H$. Hence, the effective complexity scales with the strength of correlation ρ between priors and ground-truth labels. This parallels results on hypothesis space reduction via domain knowledge [21]. We omit the full proofs because of space limitations. \square

3.3. Physics-Informed HSV Supervision

We incorporate domain-specific color priors through HSV color space analysis, thus, leveraging the physical properties of water spectral signatures. For each pixel (i, j) , we convert the RGB values to HSV representation (H_{ij}, S_{ij}, V_{ij}) and compute a physics-informed water likelihood:

$$P_{HSV}(i, j) = \sigma(\alpha_H H_{ij} + \alpha_S S_{ij} + \alpha_V V_{ij} + \beta) \quad (3)$$

where $\sigma(\cdot)$ is the sigmoid function, $\{\alpha_H, \alpha_S, \alpha_V, \beta\}$ are learnable coefficients that capture the statistical relationship between HSV values and water presence, and $P_{HSV}(i, j) \in [0, 1]$ represents the HSV-based water probability. The HSV-guided supervision loss is then formulated as:

$$\mathcal{L}_{HSV} = \frac{1}{HW} \sum_{i=1}^H \sum_{j=1}^W |m_{ij} - P_{HSV}(i, j)|^2 \cdot w_{ij} \quad (4)$$

where $m_{ij} = M_{ij}$ is the predicted water probability at pixel (i, j) , and w_{ij} is an adaptive confidence weight defined as:

$$w_{ij} = \exp\left(-\frac{d_{HSV}(i, j)^2}{2\sigma^2}\right) \quad (5)$$

where $d_{HSV}(i, j)$ measures the Euclidean distance from pixel (i, j) to the optimal water representation, σ is a bandwidth

parameter controlling the sensitivity of the weighting function, and w_{ij} assigns higher importance to pixels with strong water-like HSV signatures.

3.4. Geometric Coastline Regularization

To enforce geometric consistency and topological coherence in coastline predictions, we introduce two complementary regularization terms that address different aspects of boundary quality. We first extract candidate coastline pixels through morphological operations, computing the coastline pixel set:

$$\mathbf{C} = \text{Dilate}(\mathbf{M}, k) - \text{Erode}(\mathbf{M}, k), \quad (6)$$

where $\text{Dilate}(\cdot, k)$ and $\text{Erode}(\cdot, k)$ are morphological dilation and erosion operations, k is the size of the structuring element (typically $k = 3$ for a 3×3 kernel), and \mathbf{C} represents the set of boundary pixels between water and land regions. To ensure geometric consistency, we penalize irregular gradient fluctuations through a smoothness regularization term:

$$\mathcal{L}_{Coast} = \frac{1}{|\mathbf{C}|} \sum_{(i,j) \in \mathbf{C}} \|\nabla \mathbf{M}(i, j)\|_2^2, \quad (7)$$

where $|\mathbf{C}|$ is the cardinality of the coastline pixel set, $\nabla \mathbf{M}(i, j) = [\frac{\partial \mathbf{M}}{\partial x}, \frac{\partial \mathbf{M}}{\partial y}]_{(i,j)}$ is the spatial gradient of the mask at pixel (i, j) , and $\|\cdot\|_2$ denotes the L_2 norm. This term encourages smooth transitions, effectively reducing jagged artifacts and promoting natural coastline curvature.

Furthermore, we enforce topological consistency by penalizing columns with multiple disconnected water regions through a connectivity constraint:

$$\mathcal{L}_{Conn} = \sum_{x=1}^W \max\left(0, \frac{\text{ConnectedRegions}(\mathbf{M}[:, x]) - 1}{\text{MaxRegions}}\right) \quad (8)$$

where $\mathbf{M}[:, x]$ represents the x -th column of the water mask, $\text{ConnectedRegions}(\cdot)$ counts the number of connected components in a 1D binary sequence, MaxRegions is a normalization factor preventing unbounded loss values, and the $\max(0, \cdot)$ operation ensures non-negative penalties.

3.5. Regional Consistency Enforcement

To promote spatial homogeneity in large water bodies and reduce prediction noise within uniform regions, we introduce a variance-based sea cleanup regularizer:

$$\mathcal{L}_{Sea} = \frac{1}{|\mathbf{S}|} \sum_{(i,j) \in \mathbf{S}} \text{Var}(\mathbf{M}[\mathcal{N}(i, j)]) \quad (9)$$

where \mathbf{S} denotes the set of detected sea pixels (identified through connected component analysis with area thresholding), $\mathcal{N}(i, j)$ represents a local neighborhood around pixel (i, j) (typically a 5×5 window), $\mathbf{M}[\mathcal{N}(i, j)]$ extracts the mask values within the neighborhood, and $\text{Var}(\cdot)$ computes the statistical variance.

3.6. Unified Robust Objective

All components are integrated into a single robust objective function that balances multiple complementary aspects of coastline quality:

$$\begin{aligned} \mathcal{L}_{Robust} = & \lambda_{CE} \mathcal{L}_{CE} + \lambda_{HSV} \mathcal{L}_{HSV} \\ & + \lambda_{Coast} \mathcal{L}_{Coast} + \lambda_{Conn} \mathcal{L}_{Conn} + \lambda_{Sea} \mathcal{L}_{Sea} \end{aligned} \quad (10)$$

where \mathcal{L}_{CE} is the standard pixel-wise cross-entropy loss for semantic segmentation, defined as:

$$\mathcal{L}_{CE} = -\frac{1}{HW} \sum_{i=1}^H \sum_{j=1}^W [y_{ij} \log(m_{ij}) + (1 - y_{ij}) \log(1 - m_{ij})] \quad (11)$$

where $y_{ij} \in \{0, 1\}$ is the ground truth label for pixel (i, j) , and $\{\lambda_{CE}, \lambda_{HSV}, \lambda_{Coast}, \lambda_{Conn}, \lambda_{Sea}\}$ are coefficients that control the relative importance of each loss component.

The unified objective strategically balances four fundamental aspects of robust coastline detection: semantic fidelity through \mathcal{L}_{CE} ensures accurate pixel-level classification, spectral consistency via \mathcal{L}_{HSV} incorporates physics-informed color priors, geometric regularity enforced by \mathcal{L}_{Coast} and \mathcal{L}_{Conn} promotes smooth and topologically consistent coastlines, and regional uniformity achieved through \mathcal{L}_{Sea} maintains spatial coherence in homogeneous regions.

4. EXPERIMENTAL EVALUATION

4.1. Datasets

Experiments are conducted on coastal imagery from St Andrews region, Scotland, acquired via Sentinel-2 satellite images from May 2017 to May 2025. The dataset comprises 954 high-resolution images with pixel-level water segmentation annotations. Images utilize NIR-Red-Green band combination for enhanced water-land contrast. Dataset split: 80% training, 20% validation with stratified sampling. We compare Robust U-Net against the Traditional U-Net with identical architecture but standard cross-entropy loss without robust enhancements. This isolates the contribution of our proposed components.

4.2. Quantitative Results and Ablation Studies

Fig. 1 highlights both the individual and overall benefits of the enhancement framework. Sub-figure (a) shows that HSV-guided supervision yields the strongest impact (0.85), followed by gradient-based coastline optimization (0.79) and morphological refinement (0.74), while connectivity control (0.68) and sea cleanup (0.72) provide additional stability. Fig. 2 (a) and (b) confirm that the Robust U-Net converges as fast as the baseline while achieving higher accuracy and IoU with significantly reduced variance (from 7.9×10^{-3} to

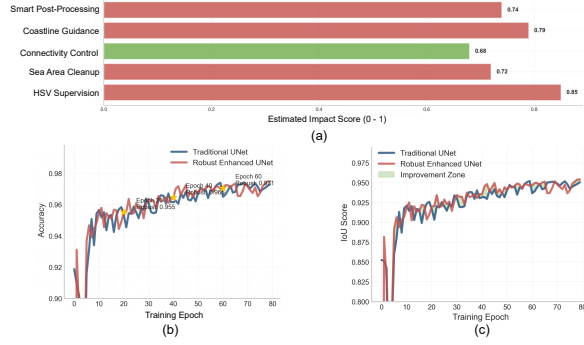


Fig. 1. Comprehensive ablation and training curves.

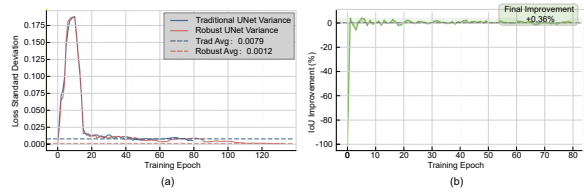


Fig. 2. Evaluation of the proposed robust enhancement framework.

1.2×10^{-3} , an 84% drop). Sub-figure (d) further shows a stable IoU gain of +0.36% in later epochs, demonstrating that the integrated constraints improve not only accuracy but also training stability and reliability.

4.3. Qualitative Robustness Analysis

As illustrated in Fig. 3, the Robust U-Net consistently outperforms the traditional U-Net across temporal scenes. While the baseline often suffers from inaccurate segmentation of vegetation or farmland as water, broken or disconnected coastlines, and unstable predictions under seasonal or illumination changes, our framework produces smoother and more continuous shoreline boundaries, effectively suppresses false positives, and preserves realistic connectivity.

4.4. Comparison with other benchmarks

Robust U-Net is further enhanced with dropout regularization, multi-scale dilated convolutions, channel and spatial attention, and Kaiming initialization for improved stability. As shown in Fig. 4, these modifications lead to faster convergence, lower training and validation loss, and consistently superior segmentation accuracy compared to DeepLabV3+ and YOLO-SEG. The Robust U-Net achieves stable IoU around 0.95–0.96 and F1-scores above 0.98, clearly outperforming the less stable DeepLabV3+ and the volatile YOLO-SEG. This confirms that attention mechanisms and multi-scale features substantially improve both convergence and generalization in coastal water segmentation; models’ performances

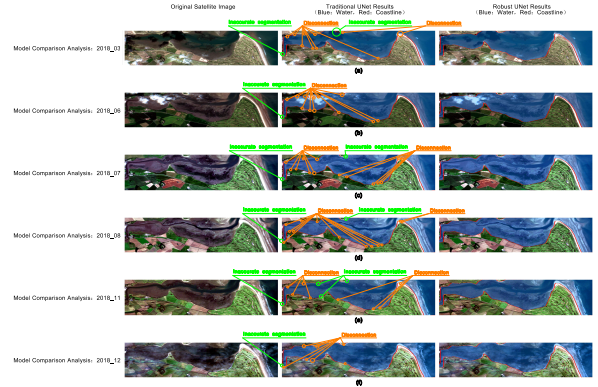


Fig. 3. Segmentation examples comparison between the proposed Robust U-Net and vanilla U-Net.

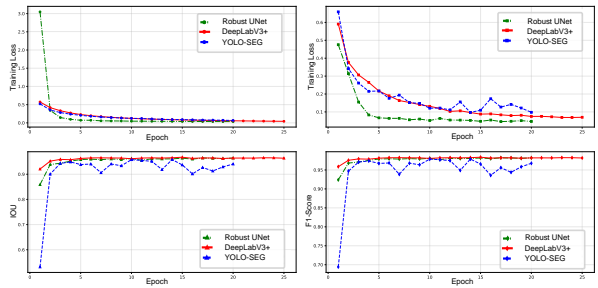


Fig. 4. Training results comparison with popular benchmarks.

are shown in Table 1.

Table 1. Evaluation Results among Different Models

Model	IoU	F1	Acc
Robust U-Net	0.9645 ± 0.003	0.9819 ± 0.002	0.9810 ± 0.002
DeepLabV3+	0.9639 ± 0.005	0.9816 ± 0.003	0.9806 ± 0.003
YOLO-SEG	0.9407 ± 0.076	0.9676 ± 0.046	0.9684 ± 0.040

5. CONCLUSIONS

We introduce a robust framework for coastal water segmentation that integrates HSV-guided supervision, geometric and morphological constraints, and sea cleanup regularization. Theory and experiments show improved stability, faster convergence, and higher accuracy over baselines. Robust U-Net achieves the best performance (IoU 0.9645, F1 0.9819, accuracy 0.9810) with more reliable boundaries. Future work includes multimodal fusion and dynamic monitoring.

Acknowledgment

This work is partially funded by the EU TERRA # 101189962.

6. REFERENCES

- [1] Freya ME Muir et al., “Vedgesat: An automated, open-source toolkit for coastal change monitoring using satellite-derived vegetation edges,” *Earth Surface Processes and Landforms*, vol. 49, no. 8, pp. 2405–2423, 2024.
- [2] Jair E Garcia et al., “Differentiating biological colours with few and many sensors: spectral reconstruction with rgb and hyperspectral cameras,” *PLoS One*, vol. 10, no. 5, pp. e0125817, 2015.
- [3] Heidi M Dierssen et al., “Living up to the hype of hyperspectral aquatic remote sensing: science, resources and outlook,” *Frontiers in Environmental Science*, vol. 9, pp. 649528, 2021.
- [4] Nanyang Yan, Zhen Sun, Wei Huang, Zhao Jun, and Shaojie Sun, “Assessing landsat-8 atmospheric correction schemes in low to moderate turbidity waters from a global perspective,” *International Journal of Digital Earth*, vol. 16, no. 1, pp. 66–92, 2023.
- [5] Chen Wu et al., “Unet-like remote sensing change detection: A review of current models and research directions,” *IEEE Geoscience and Remote Sensing Magazine*, 2024.
- [6] Zhouyayan Li and Ibrahim Demir, “U-net-based semantic classification for flood extent extraction using sar imagery and gee platform: A case study for 2019 central us flooding,” *Science of The Total Environment*, vol. 869, pp. 161757, 2023.
- [7] Jiansen Zhao et al., “Improved unet-based shoreline detection method in real time for unmanned surface vehicle,” *Journal of Marine Science and Engineering*, vol. 11, no. 5, pp. 1049, 2023.
- [8] Mohammed Attya, OM Abo-Seida, HM Abdulkader, and Amgad M Mohammed, “A hybrid deep learning approach for accurate water body segmentation in satellite imagery,” *Earth Science Informatics*, vol. 18, no. 2, pp. 418, 2025.
- [9] Amira S Mahmoud, Sayed A Mohamed, Ashraf K Helmy, and Ayman H Nasr, “Bdcn_unet: Advanced shoreline extraction techniques integrating deep learning,” *Earth Science Informatics*, vol. 18, no. 2, pp. 187, 2025.
- [10] Ray Wang, Tahiya Chowdhury, and Alejandra C Ortiz, “Semantic segmentation framework for atoll satellite imagery: An in-depth exploration using unet variants and segmentation gym,” *Applied Computing and Geosciences*, vol. 25, pp. 100217, 2025.
- [11] Ali Gonzalez-Perez et al., “Deep and machine learning image classification of coastal wetlands using unpiloted aircraft system multispectral images and lidar datasets,” *Remote Sensing*, vol. 14, no. 16, pp. 3937, 2022.
- [12] Yuhao Qing, Liquan Shen, Zhijun Fang, and Yueying Wang, “Hg2former: Hsv-gamma guided transformers for efficient underwater image enhancement,” *IEEE Journal of Oceanic Engineering*, 2025.
- [13] Mohammed R Mahmood, Baydaa Ismail Abraham, Huda J Jumaah, Hayder A Alalwan, and Malik M Mohammed, “Drought monitoring of large lakes in iraq using remote sensing images and normalized difference water index (ndwi),” *Results in Engineering*, vol. 25, pp. 103854, 2025.
- [14] Eduardo Felix Justiniano et al., “A new spectral index for mapping water surfaces in urban contexts,” *IEEE Journal of Selected Topics in Applied Earth Observations and Remote Sensing*, 2025.
- [15] Dong Liu et al., “Mim-unet: An efficient building image segmentation network integrating state space models,” *Alexandria Engineering Journal*, vol. 120, pp. 648–656, 2025.
- [16] Naga Surekha Jonnala, Renuka Chowdary Bheemana, Krishna Prakash, Shonak Bansal, Arpit Jain, Vaibhav Pandey, Mohammad Rashed Iqbal Faruque, and KS Al-Mugren, “Dsia u-net: deep shallow interaction with attention mechanism unet for remote sensing satellite images,” *Scientific Reports*, vol. 15, no. 1, pp. 549, 2025.
- [17] Qiang Gao et al., “Msfm-unet: enhancing medical image segmentation with multi-scale and multi-view frequency fusion,” *Pattern Analysis and Applications*, vol. 28, no. 1, pp. 17, 2025.
- [18] Yuzeng Chen et al., “Hyperspectral video tracking with spectral-spatial fusion and memory enhancement,” *IEEE Transactions on Image Processing*, 2025.
- [19] Putri Fausyah Johari et al., “Corn leaf diseases classification using cnn with glcm, hsv, and l* a* b* features,” *Jurnal Teknik Informatika (Jutif)*, vol. 6, no. 2, pp. 709–722, 2025.
- [20] Saeed Ghadimi and Guanghui Lan, “Stochastic first- and zeroth-order methods for nonconvex stochastic programming,” *SIAM Journal on Optimization*, vol. 23, no. 4, pp. 2341–2368, 2013.
- [21] Ting Yu, Tony Jan, Simeon Simoff, and John Debenham, “Incorporating prior domain knowledge into inductive machine learning,” *International Journal of Artificial Intelligence Tools*, vol. 16, no. 03, pp. 341–357, 2007.